JACS
JOURNAL OF THE AMERICAN CHEMICAL SOCIETY
Communication
pubs.acs.org/JACS

New Heterometallic Zirconium Metalloporphyrin Frameworks and Their Heteroatom-Activated High-Surface-Area Carbon Derivatives

Qipu Lin,[†] Xianhui Bu,*[,‡] Aiguo Kong,[†] Chengyu Mao,[†] Xiang Zhao,[†] Fei Bu,[†] and Pingyun Feng*[,†]

[†]Department of Chemistry, University of California, Riverside, California 92521, United States
[‡]Department of Chemistry and Biochemistry, California State University, Long Beach, California 90840, United States

Supporting Information

ABSTRACT: Four cubic zirconium-porphyrin frameworks, CPM-99(H_2, Zn, Co, Fe), were synthesized by a molecular-configuration-guided strategy. Augmentation of *meso*-substituted side arms (with double-torsional biphenyl rings) of tetratopic porphyrin linkers leads to a successful implementation of zirconium-carboxylate frameworks with cubic 2.5 nm cage. The hard-templating effect of Zr_6-polyoxo-cluster and uniformly embedded (metallo)-porphyrin centers endow CPM-99 with highly desirable properties as precursors for oxygen reduction reaction (ORR) catalysts. The pyrolytic products not only retain the microcubic morphology of the parent CPM-99 but also possess porphyrinic active sites, hierarchical porosity, and highly conducting networks. CPM-99Fe-derived material, denoted CPM-99Fe/C, exhibits the best ORR activity, comparable to benchmark 20% Pt/C in alkaline and acidic media, but CPM-99Fe/C is more durable and methanol-tolerant. This work demonstrates a new route for the development of nonprecious metal ORR catalysts from stable metalloporphyrinic MOFs.

Metal−organic frameworks based on zirconium (Zr-MOFs) have attracted increasing attention since the first report of UiO-66 built of 12-connected $[Zr_6(\mu_3\text{-}O)_4(\mu_3\text{-}OH)_4(O_2C)_{12}]$ cluster and terephthalic acid and its isoreticular series.[1] Recently, efforts have been extended to other ligand types such as bent dicarboxylates or polytopic ligands.[2] Compared to other MOFs, an outstanding feature of Zr-MOFs is their exceptional stability.[3] However, so far only a small number of Zr-MOFs have been made, in part because of the difficulty in growing large-enough single crystals for structural studies.[1a]

Metalloporphyrins are found in nature as light harvesters, oxygen carriers, and biocatalysts. So, their incorporation into MOFs can greatly enrich the MOF functionalities.[4] Indeed, high porosity, ultrastability, and uniform distribution of catalytic sites have made zirconium-(metallo)porphyrin frameworks (ZPFs) of interest for potential applications in gas storage, biomimetic catalysis, and clean energy.[5] The latest studies of the ZPFs have led to the growth and characterization of single crystalline materials built of Zr_6 clusters usually with reduced connectivity (8 or 6).[5,6] A closer examination reveals that the reduction in connectivity is due to the symmetry mismatch between 12-connected Zr_6-cuboctahedron and 4 noncoplanar benzoic groups of the commercially available tetrakis(4-carboxyphenyl)-porphyrin (= TCPP) spacer. Since the higher connectivity often contributes to the greater stability,[7] it is of interest to design new (metallo)porphyrin ligands that could take the full advantage of the 12-connectedness of Zr_6-cuboctahedron.

An emerging application that could benefit from enhanced stability of MOFs is their use as precursors for the synthesis of electrocatalysts for oxygen reduction reaction (ORR), because the resulting carbonized catalysts are more likely to retain the high surface area of their less-collapse-prone precursors. ORR is generally performed with Pt catalysts, however, new catalysts based on earth-abundant elements are highly desirable.[8] Noble-metal-free electrocatalysts prepared from zeolitic imidazolate frameworks (ZIFs) were found to show promising catalytic performances.[9] The $Co(Zn)N_4$ units in ZIFs allow doping of the resulting carbon frameworks with metal and nitrogen to boost the catalytic activity.[10]

In comparison with ZIFs, porphyrin-MOFs have rarely been used as precursor to make porphyrinic carbon, but they are expected to have some advantages over ZIFs. For example, so far ZIFs have only been made with a limited number of metal types (e.g., Zn, Co, and Cd),[11] whereas porphyrin-MOFs can contain more diverse metal types and oxidation states. In fact, framework stability and active site insertion are two main concerns in the selection of precursors for ORR.[8c,12] As shown here, ZPFs can excel in both aspects, because unlike tetrahedral coordination of Zn/Co in ZIFs, macrocyclic effect allows better encapsulation of metals in porphyrins.

Here, by restoring coplanarity of four carboxyl groups through reverse rotation of an extra inserted phenyl group in each arm of the parent TCPP ligand, a series of ZPFs have been made.[13] These ultrastable, single-crystalline ZPFs can be made with or without secondary metal ions and are denoted as CPM-99X (CPM = crystalline porous material, X = H_2, Zn, Co, Fe). They feature a binodal cubic net composed of 12-connected $Zr_6O_4(OH)_4$ cuboctahedra linked by longer tetrakis(4-carboxybiphenyl)porphyrin (TCBPP). The porphyrinic characteristics as well as cube morphology were retained in the carbonized composites. The ORR studies show that the optimized iron-porphyrinic carbon (denoted CPM-99Fe/C), derived by carbonization of CPM-99Fe at 700 °C, exhibits the excellent ORR activity comparable to the commercial benchmark 20% Pt/C in both alkaline and acidic media.

Solvothermal reactions of TCBPP-X (X = H_2, Zn, Co, Fe), $ZrOCl_2{\cdot}8H_2O$ and benzoic acid in *N*,*N*-diethylformamide for 5 days at 120 °C yielded single crystals of CPM-99 series. With the

Received: January 5, 2015
Published: February 4, 2015

DOI: 10.1021/jacs.5b00076
J. Am. Chem. Soc. 2015, 137, 2235−2238

size of ~0.20 mm, black cube-shaped crystals (Figure 1e) allowed the structure determination by single-crystal X-ray diffraction.

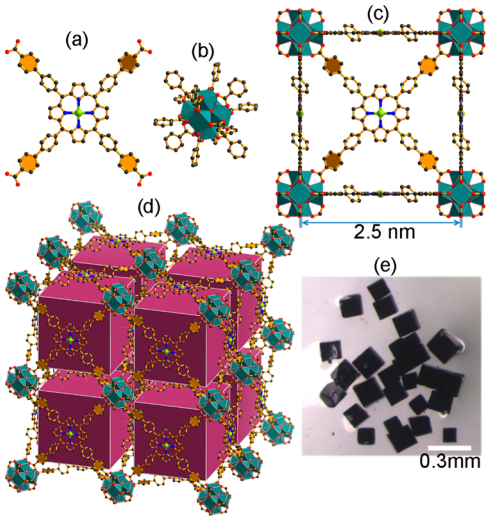

Figure 1. (a) Augmented tetracarboxylic porphyrinic linkers, TCBPP-X (X = H_2, Zn, Co, Fe). (b) 12-connected $Zr_6(\mu_3\text{-}O)_4(\mu_3\text{-}OH)_4(O_2C)_{12}$ cluster. (c) Cubic cage with 2.5 nm edge length. (d) The 3D network with Zr_6 clusters shown as polyhedra and 3D cubic-cavity packing in CPM-99Fe. Color scheme: Zr (teal); Fe (lime); O (red); N (blue); C (gray). (e) Photograph of CPM-99Fe.

The 3D framework contains large cubic cages with an edge length as large as 2.5 nm (Figure 1c), which is among the largest known in noninterpenetrated cube-based MOFs.[14] Each Zr_6 cluster resides on one vertex and each face of the cube is capped by one square TCBPP spacer. Such nanocubic cavities are packed in a primitive cubic lattice (Figure 1d). Apart from the cubic cage, the **ftw**-typed structure possesses another kind of cage, slightly distorted octahedron with a cavity diameter of ~1.1 nm, comprising two Zr_6 clusters in the axial sites and four TCBPP ligands in the equatorial plane. In general, the pore size expansion for cubic structures through the longer building unit leads to lower framework stability and, in many cases, less desired interpenetration.[14a,15] Interestingly, interpenetration is avoided in CPM-99 with **ftw** topology, while the high stability is retained.

For CPM-99Fe, the PLATON-calculated solvent accessible volume is 82%, indicating its highly porous nature. Despite such large pores, it is resistant to heat treatment. After degassing at 200°, powder X-ray diffraction (PXRD) patterns (Figure S14) remained nearly unchanged. Thermogravimetric analysis under nitrogen flow indicates that CPM-99Fe possesses high thermal stability up to about 450 °C. The porosity of CPM-99X was examined by nitrogen adsorption at 77 K. As a representative example, the quasi-type IV isotherm of CPM-99Fe exhibits the second increase at P/P_0 = 0.02, suggesting borderline mesoporosity. A N_2 uptake of 450 cm^3g^{-1} (STP) and a Brunauer–Emmett–Teller (BET) surface area of 1030 $m^2\ g^{-1}$ were observed (much lower than the theoretical value of 3324 $m^2\ g^{-1}$, possibly due to incomplete activation and/or potential defects in the sample). The evaluation by the density functional theory using the N_2 sorption curve indicates that there are two types of pores, with sizes of 19 and 9 nm, attributable to cubic and pseudo-octahedral cavities, respectively, which are consistent with the crystallographic data when van der Waals contact is considered. Other CPM-99 materials with different metal-loporphyrin centers showed similar results (Figure S28). The CO_2 uptakes at 273 K for CPM-99(H_2, Zn, Co and Fe) were found to be 73, 60, 61, and 76 $cm^3\ g^{-1}$, respectively (Figure 2a),

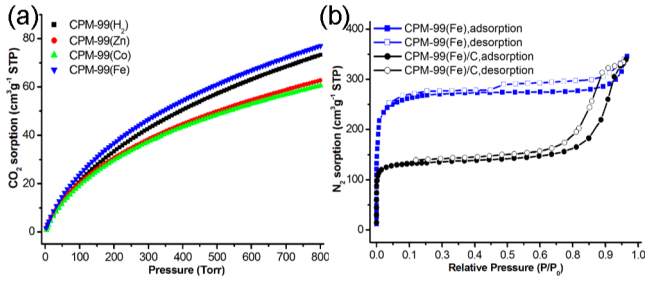

Figure 2. (a) CO_2 adsorption isotherms of CPM-99X series at 273 K. (b) N_2 sorption isotherms of CPM-99Fe and CPM-99Fe/C at 77K.

which are at the high end among zirconium and/or porphyrin-based MOFs.[16] The similar isosteric heats of adsorption (Q_{st}) toward CO_2 for the CPM-99 family indicate a limited effect of the porphyrinic metal center on the gas uptake. However, the nature of porphyrinic-metal sites greatly influence their ORR catalytic properties as described below.

As shown above, CPM-99X exhibits desirable features for serving as the precursor in the synthesis of the efficient ORR catalysts. Thus, carbonization was performed to convert the crystals of CPM-99X into (metallo)porphyrinic carbons, denoted as CPM-99X/C (X = H_2, Zn, Co, Fe; the detailed procedure in SI). A comparative study shows that CPM-99Fe/C exhibits the highest catalytic efficiency and is therefore described below in detail. The optimum annealing temperature was found to be 700 °C, and PXRD data exhibit peaks at ~25 and 44° corresponding to the diffractions from the (002) and (100) graphitic carbon planes, respectively, suggesting the presence of long-range ordering in the carbon matrix. In addition to the graphitic peaks, the pronounced diffraction peaks (much sharper for samples treated at the elevated temperature such as 800 and 900 °C), matching the cubic ZrO_2 (JCPDS card 27-0997), were also observed. After leaching with dilute HF (5 wt % in water), no PXRD signals of the zirconia residues were found. This observation was further supported by the energy-dispersive X-ray and X-ray photoelectron spectroscopy (XPS). The cube morphologies of the CPM-99X/C were seen in the scanning electron microscopy (SEM) images (Figures 3b and S35). The optical properties of CPM-99X/C and CPM-99X were also studied using solid-state diffuse reflectance spectroscopy (Figures 3c, S21, and S39), indicating that the pyrolytic product did somewhat retain the porphyrinic characteristic. Moreover, the hollow cores enclosed by the lattice fringes, in agreement with the visible diffraction rings of the selected area electron diffraction pattern (Figure S38), were observed in the high-resolution transmission electron microscopy image (Figure S37). From these studies, together with the presence of mesopore detected by the N_2 sorption (see below), it may be concluded that Zr_6-polyoxo-cluster in CPM-99X serves as the hard template to impede the agglomeration of the resulting electrocatalytic nanofragments and helps create the nanoscale cavity upon removal by acid wash.

N_2 adsorption–desorption isotherms at 77 K for CPM-99Fe/C showed a steep increase at low relative pressures, demonstrating microporous characteristics (the BET surface area of 399 $m^2\ g^{-1}$). The slight hysteresis of the desorption isotherm at high relative pressure suggests the presence of mesopores centered at 3.8 nm as calculated from the desorption

DOI: 10.1021/jacs.5b00076
J. Am. Chem. Soc. 2015, 137, 2235–2238

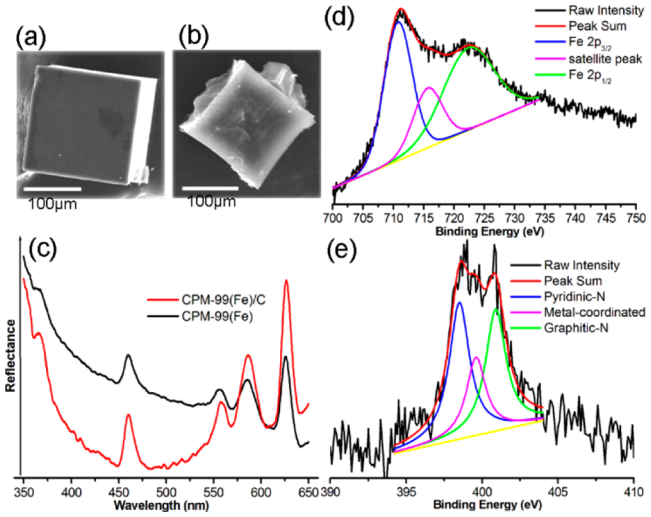

Figure 3. (a,b) SEM images for CPM-99Fe and CPM-99Fe/C. (c) UV–vis diffuse reflectance spectra of CPM-99Fe and CPM-99Fe/C. (d,e) XPS Fe 2p and N 1s spectra of the CPM-99Fe/C.

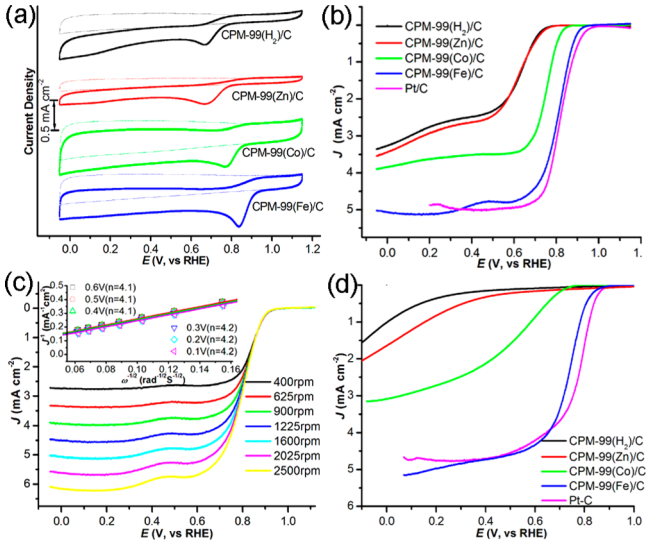

Figure 4. (a) CVs and (b) RDE polarization curves on CPM-99X/C and 20% Pt/C in 0.1 M KOH solution. (c) RDE polarization curves on CPM-99Fe/C at different rotation rates. Inset: K-L plot of J^{-1} vs ω^{-1} at different potentials. (d) RDE polarization curves on CPM-99X/C and 20% Pt/C in 0.1 M $HClO_4$ solution. The catalyst loadings on the electrodes were 0.2 (in KOH) or 0.6 (in $HClO_4$) mg·cm^{-2} for the CPM-99X/C and 0.1 mg·cm^{-2} for Pt/C (20 wt %, Alfa). The scan rate is 10 mV·s^{-1}.

isotherm using the Barrett–Joyner–Halenda model. The surface chemistry is of particular interest, and the electronic states of Fe, N, and C were examined by XPS measurements (Figure S40). As shown in Figure 3d (high-resolution Fe 2p XPS spectrum), $2p_{3/2}$ and $2p_{1/2}$ peaks occur at 710.8 and 722.9 eV, respectively, which match well with those for Fe(II).[12c] The N 1s spectrum (Figure 3e) is deconvoluted into three peaks at 398.5, 399.6, and 400.9 eV, corresponding to pyridinic, metal-coordinated, and graphitic nitrogen species, respectively.[12b,17] Based on these data, the Fe ions are believed to be associated with N atoms to form catalytically active sites.[18] In addition, the C 1s peaks for the CPM-99Fe/C porous carbon were centered at ~285 eV (Figure S41) and were slightly asymmetric, which is a common characteristic for nitrogen-doped graphitic carbon.[12a]

To assess the electrocatalytic performance of the CPM-99-derived materials in comparison to the benchmark carbon supported Pt (viz. 20% Pt/C, Alfa), ORR activities were evaluated using standard 3-electrode half-cell setup, and cyclic voltammetry (CV), rotating ring electrode (RDE) polarization, and chronoamperometric measurements were performed. All potentials refer to the reversible hydrogen electrode scale. Prior to each experiment, the electrolytes were saturated with O_2 or Ar, respectively. In an Ar-saturated solution of 0.1 M KOH, the CV curves within the entire potential range showed a featureless slope for the cathodic current. In contrast, when the electrolyte was saturated by O_2, the well-defined cathodic ORR peaks were observed, illustrating their effective ORR activities in alkaline medium. Among the four samples, CPM-99Fe/C shows an ORR peak at the most positive potential of 0.836 V. The electrocatalytic activities of CPM-99X/C are in the order: Fe > Co > Zn ≈ H_2 (Figure 4a), supported by the linear sweep voltammetry measurements on a RDE. As shown in Figure 4b, CPM-99Fe/C displays the best ORR activity among the CPM-99-derived electrodes, exhibiting the onset and half-wave potential (0.950 and 0.802 V, determined at the polarization curves at 1600 rpm) close to those (0.978 and 0.818 V) of the 20 wt % Pt/C. These results reveal that CPM-99Fe/C has the ORR catalytic activity comparable to commercial Pt/C catalyst.

Moreover, the Koutecky–Levich (K-L) plots from RDE polarization curves (Figure 4c) for CPM-99Fe/C between 0.6 and 0.1 V exhibited good parallel straight lines, and the number of electron being transferred was calculated to be 4.1(±0.1), meaning that CPM-99Fe/C catalyzed a 4-electron ORR in 0.1 M KOH solution. However, the slopes of plots for CPM-99Co/C indicated that the electron-transfer number at 0.4 V is 3.2, suggesting a mixed 4- and 2-electron-transfer process of ORR. On CPM-99Zn/C and CPM-99H_2/C electrodes 2-electron ORR process dominates, as their electron numbers transferred per O_2 further reduced to 2.6 and 2.3, respectively (Figure S46). The CPM-99Fe/C catalyst exhibits long-term durability, superior to Pt/C (Figure S47). Through continuous potential cycling, the deterioration of CPM-99Fe/C after 10000 cycles resulted in a slight peak current decrease with a retention of ~93% (at cathodic peak, SI). The CPM-99Fe-derived electrode was nearly free from the methanol crossover effect, which is different from the significant impact of methanol on Pt/C catalyst. Its durability is higher than Pt/C catalysts (with retention index of 75.3%) and many nonprecious metal catalysts at the similar measurement conditions.

In addition to the basic medium (0.1 M KOH), the ORR performance of the CPM-99-derived electrodes in O_2-saturated acidic medium (0.1 M $HClO_4$ electrolyte) was investigated. Again, the CPM-99Fe/C-electrode showed the best electrocatalytic activity among four samples, with an onset potential (0.875 V) comparable to the Pt/C (0.880 V), while the CPM-99Co/C, CPM-99Zn/C and CPM-99H_2/C electrodes exhibited much lower onset potential and current density (Figure 4d). The CPM-99X/C electrodes in the acid solution showed the same activity sequence (Fe > Co > Zn ≈ H_2) and were also free from the methanol crossover effect. Based on the K-L equation, the transferred electron number per O_2 molecule for the CPM-99Fe/C in the acidic medium was calculated to be 4.0(±0.1) (Figure S52), suggesting a 4-electron ORR pathway even in the acid condition. The prominent performance of CPM-99Fe-derived electrode is believed to come from unique structural and compositional features of its precursor, such as high porosity,

DOI: 10.1021/jacs.5b00076
J. Am. Chem. Soc. 2015, 137, 2235–2238

high thermal stability, uniform distribution of FeN_4 active sites, and hard-templating effects by the rigid framework.

In summary, we have described a molecular-configuration-based materials design strategy for fabricating a series of noninterpenetrating ZPFs with nanoscale cubic cavity. The resulting high porosity and stability, coupled with uniformly decorated pore walls by FeN_4 macrocyclic dyes, make such materials well suited as single precursor (i.e., without additional metal species or nitrogen/carbon sources) for synthesizing highly active nonprecious metal catalysts for the ORR. CPM-99Fe-derived carbonization product exhibited high ORR activity (with onset potential of 0.950 and 0.875 V in alkaline and acidic electrolytes, respectively) comparable to 20% Pt/C catalyst (0.978 and 0.880 V, respectively). The efficient electrocatalytic activity of nanocomposite CPM-99Fe/C can be attributed to its unique precursor with large cavity, high proportion of heme-like center and hard polyoxozirconate cluster template. This work demonstrates a successful implementation of rational design of porphyrin-functionalized zirconium-carboxylate frameworks with desired topology and porosity and reveals a new strategy for developing high-performance electrocatalysts.

■ ASSOCIATED CONTENT

Supporting Information

Experimental details, characterization data, crystallographic data (CIF files, CCDC#1044848−1044851), and additional tables and figures. This material is available free of charge via the Internet at http://pubs.acs.org.

■ AUTHOR INFORMATION

Corresponding Authors

*pingyun.feng@ucr.edu
*xianhui.bu@csulb.edu

Notes

The authors declare no competing financial interest.

■ ACKNOWLEDGMENTS

The research was supported by the U.S. Department of Energy, Office of Basic Energy Sciences, Division of Materials Sciences and Engineering under award no. DE-FG02-13ER46972.

■ REFERENCES

(1) (a) Cavka, J. H.; Jakobsen, S.; Olsbye, U.; Guillou, N.; Lamberti, C.; Bordiga, S.; Lillerud, K. P. *J. Am. Chem. Soc.* **2008**, *130*, 13850. (b) Kandiah, M.; Nilsen, M. H.; Usseglio, S.; Jakobsen, S.; Olsbye, U.; Tilset, M.; Larabi, C.; Quadrelli, E. A.; Bonino, F.; Lillerud, K. P. *Chem. Mater.* **2010**, *22*, 6632. (c) Schaate, A.; Roy, P.; Godt, A.; Lippke, J.; Waltz, F.; Wiebcke, M.; Behrens, P. *Chem.—Eur. J.* **2011**, *17*, 6643. (d) Katz, M. J.; Brown, Z. J.; Colon, Y. J.; Siu, P. W.; Scheidt, K. A.; Snurr, R. Q.; Hupp, J. T.; Farha, O. K. *Chem. Commun.* **2013**, *49*, 9449. (e) Shen, L.; Liang, S.; Wu, W.; Liang, R.; Wu, L. *J. Mater. Chem. A* **2013**, *1*, 11473. (f) Shen, L.; Wu, W.; Liang, R.; Lin, R.; Wu, L. *Nanoscale* **2013**, *5*, 9374. (g) Shearer, G. C.; Chavan, S.; Ethiraj, J.; Vitillo, J. G.; Svelle, S.; Olsbye, U.; Lamberti, C.; Bordiga, S.; Lillerud, K. P. *Chem. Mater.* **2014**, *26*, 4068. (h) Cliffe, M. J.; Wan, W.; Zou, X.; Chater, P. A.; Kleppe, A. K.; Tucker, M. G.; Wilhelm, H.; Funnell, N. P.; Coudert, F. X.; Goodwin, A. L. *Nat. Commun.* **2014**, *5*, 4176.

(2) (a) Zhang, M.; Chen, Y. P.; Bosch, M.; Gentle, T., 3rd; Wang, K.; Feng, D.; Wang, Z. U.; Zhou, H. C. *Angew. Chem., Int. Ed.* **2014**, *53*, 815. (b) Furukawa, H.; Gandara, F.; Zhang, Y. B.; Jiang, J.; Queen, W. L.; Hudson, M. R.; Yaghi, O. M. *J. Am. Chem. Soc.* **2014**, *136*, 4369. (c) Wei, Z.; Gu, Z. Y.; Arvapally, R. K.; Chen, Y. P.; McDougald, R. N., Jr.; Ivy, J. F.; Yakovenko, A. A.; Feng, D.; Omary, M. A.; Zhou, H. C. *J. Am. Chem. Soc.* **2014**, *136*, 8269.

(3) Wu, H.; Yildirim, T.; Zhou, W. *J. Phys. Chem. Lett.* **2013**, *4*, 925.

(4) (a) Pan, L.; Kelly, S.; Huang, X.; Li, J. *Chem. Commun.* **2002**, 2334. (b) Zou, C.; Zhang, Z.; Xu, X.; Gong, Q.; Li, J.; Wu, C. D. *J. Am. Chem. Soc.* **2012**, *134*, 87. (c) Fateeva, A.; Chater, P. A.; Ireland, C. P.; Tahir, A. A.; Khimyak, Y. Z.; Wiper, P. V.; Darwent, J. R.; Rosseinsky, M. J. *Angew. Chem., Int. Ed.* **2012**, *51*, 7440. (d) Son, H. J.; Jin, S.; Patwardhan, S.; Wezenberg, S. J.; Jeong, N. C.; So, M.; Wilmer, C. E.; Sarjeant, A. A.; Schatz, G. C.; Snurr, R. Q.; Farha, O. K.; Wiederrecht, G. P.; Hupp, J. T. *J. Am. Chem. Soc.* **2013**, *135*, 862. (e) Park, J.; Feng, D.; Yuan, S.; Zhou, H. C. *Angew. Chem., Int. Ed.* **2015**, *54*, 430.

(5) (a) Feng, D.; Gu, Z. Y.; Li, J. R.; Jiang, H. L.; Wei, Z.; Zhou, H. C. *Angew. Chem., Int. Ed.* **2012**, *51*, 10307. (b) Jiang, H. L.; Feng, D.; Wang, K.; Gu, Z. Y.; Wei, Z.; Chen, Y. P.; Zhou, H. C. *J. Am. Chem. Soc.* **2013**, *135*, 13934. (c) Feng, D.; Chung, W. C.; Wei, Z.; Gu, Z. Y.; Jiang, H. L.; Chen, Y. P.; Darensbourg, D. J.; Zhou, H. C. *J. Am. Chem. Soc.* **2013**, *135*, 17105.

(6) Morris, W.; Volosskiy, B.; Demir, S.; Gandara, F.; McGrier, P. L.; Furukawa, H.; Cascio, D.; Stoddart, J. F.; Yaghi, O. M. *Inorg. Chem.* **2012**, *51*, 6443.

(7) (a) Yuan, D.; Zhao, D.; Timmons, D. J.; Zhou, H.-C. *Chem. Sci.* **2011**, *2*, 103. (b) Zhou, Y. X.; Chen, Y. Z.; Hu, Y.; Huang, G.; Yu, S. H.; Jiang, H. L. *Chem.—Eur. J.* **2014**, *20*, 14976.

(8) (a) Jaouen, F.; Proietti, E.; Lefèvre, M.; Chenitz, R.; Dodelet, J.-P.; Wu, G.; Chung, H. T.; Johnston, C. M.; Zelenay, P. *Energy Environ. Sci.* **2011**, *4*, 114. (b) Dai, L. M. *Acc. Chem. Res.* **2013**, *46*, 31. (c) Wu, G.; Zelenay, P. *Acc. Chem. Res.* **2013**, *46*, 1878. (d) Wang, H.; Dai, H. *Chem. Soc. Rev.* **2013**, *42*, 3088. (e) Katsounaros, I.; Cherevko, S.; Zeradjanin, A. R.; Mayrhofer, K. J. *Angew. Chem., Int. Ed.* **2014**, *53*, 102.

(9) (a) Ma, S.; Goenaga, G. A.; Call, A. V.; Liu, D. J. *Chem.—Eur. J.* **2011**, *17*, 2063. (b) Aijaz, A.; Fujiwara, N.; Xu, Q. *J. Am. Chem. Soc.* **2014**, *136*, 6790. (c) Zhao, D.; Shui, J. L.; Grabstanowicz, L. R.; Chen, C.; Commet, S. M.; Xu, T.; Lu, J.; Liu, D. J. *Adv. Mater.* **2014**, *26*, 1093.

(10) (a) Wang, S. B.; Hou, Y. D.; Lin, S.; Wang, X. C. *Nanoscale* **2014**, *6*, 9930. (b) Wang, S.; Lin, J.; Wang, X. *Phys. Chem. Chem. Phys.* **2014**, *16*, 14656. (c) Wang, S.; Yao, W.; Lin, J.; Ding, Z.; Wang, X. *Angew. Chem., Int. Ed.* **2014**, *53*, 1034.

(11) (a) Park, K. S.; Ni, Z.; Cote, A. P.; Choi, J. Y.; Huang, R.; Uribe-Romo, F. J.; Chae, H. K.; O'Keeffe, M.; Yaghi, O. M. *Proc. Natl. Acad. Sci. U. S. A.* **2006**, *103*, 10186. (b) Karagiaridi, O.; Bury, W.; Sarjeant, A. A.; Stern, C. L.; Farha, O. K.; Hupp, J. T. *Chem. Sci.* **2012**, *3*, 3256.

(12) (a) Yuan, S. W.; Shui, J. L.; Grabstanowicz, L.; Chen, C.; Commet, S.; Reprogle, B.; Xu, T.; Yu, L. P.; Liu, D. J. *Angew. Chem., Int. Ed.* **2013**, *52*, 8349. (b) Wu, Z. S.; Chen, L.; Liu, J.; Parvez, K.; Liang, H.; Shu, J.; Sachdev, H.; Graf, R.; Feng, X.; Mullen, K. *Adv. Mater.* **2014**, *26*, 1450. (c) Xiang, Z.; Xue, Y.; Cao, D.; Huang, L.; Chen, J. F.; Dai, L. *Angew. Chem., Int. Ed.* **2014**, *53*, 2433.

(13) Just prior to the submission of this manuscript, a similar strategy was reported by Liu, T. F.; Feng, D.; Chen, Y. P.; Zou, L.; Bosch, M.; Yuan, S.; Wei, Z.; Fordham, S.; Wang, K.; Zhou, H. C. *J. Am. Chem. Soc.* **2015**, *137*, 413 whose work focuses on the tuning of porosity through ligand design and variation, while this work focuses on the ligand and heteroatom effect for optimizing ORR catalysts.

(14) (a) Eddaoudi, M.; Kim, J.; Rosi, N.; Vodak, D.; Wachter, J.; O'Keeffe, M.; Yaghi, O. M. *Science* **2002**, *295*, 469. (b) Chen, B.; Ockwig, N. W.; Millward, A. R.; Contreras, D. S.; Yaghi, O. M. *Angew. Chem.* **2005**, *117*, 4823.

(15) Coskun, A.; Hmadeh, M.; Barin, G.; Gandara, F.; Li, Q.; Choi, E.; Strutt, N. L.; Cordes, D. B.; Slawin, A. M.; Stoddart, J. F.; Sauvage, J. P.; Yaghi, O. M. *Angew. Chem., Int. Ed.* **2012**, *51*, 2160.

(16) (a) Gao, W. Y.; Wojtas, L.; Ma, S. *Chem. Commun.* **2014**, *50*, 5316. (b) Wang, X. S.; Meng, L.; Cheng, Q.; Kim, C.; Wojtas, L.; Chrzanowski, M.; Chen, Y. S.; Zhang, X. P.; Ma, S. *J. Am. Chem. Soc.* **2011**, *133*, 16322. (c) Gao, W. Y.; Chrzanowski, M.; Ma, S. *Chem. Soc. Rev.* **2014**, *43*, 5841.

(17) Liang, H. W.; Wei, W.; Wu, Z. S.; Feng, X.; Mullen, K. *J. Am. Chem. Soc.* **2013**, *135*, 16002.

(18) (a) Wu, J.; Li, W.; Higgins, D.; Chen, Z. *J. Phys. Chem. C* **2011**, *115*, 18856. (b) Zhao, Y.; Watanabe, K.; Hashimoto, K. *J. Am. Chem. Soc.* **2012**, *134*, 19528.

DOI: 10.1021/jacs.5b00076
J. Am. Chem. Soc. 2015, 137, 2235−2238